Quantitative PCR (qPCR) was carried out by real-time PCR using SYBR® Green I. The primer sequences and PCR conditions are shown in Supplementary Table S1. The amplification curve of a sample was compared with those of standard DNA samples with known copy numbers to obtain the copy number in the sample. The number of target cDNA molecules was normalized to those of mouse *Gapdh* cDNA molecules.

Statistical analysis

To evaluate significant difference between two independent groups of sample data, the Mann–Whitney *U*-test was used.

RESULTS

Combinations of epigenetic marks are visualized by iChmo

To visualize a combination of histone modifications, we first performed the *in situ* PLA focusing on two combinations of epigenetic marks known to be present at active loci, one H3K4me3 and H3K9ac and the other H3K4me3 and RNAPII (18). Immunofluorescence staining of mouse ESCs confirmed that the signals of H3K4me3 and H3K9ac, and those of H3K4me3 and RNAPII, were observed as merged signals in the nucleus (Figure 1A and B). The *in situ* PLA for the combinations of H3K4me3/H3K9ac and H3K4me3/RNAPII demonstrated a large number of fluorescence spots in the nucleus (Figure 1E and F). The possibility that the signals were derived from non-specific binding of PLA probes was excluded by the absence of fluorescence spots of the *in situ* PLA using antibodies against H3K4me3 and H3K9me3 that were not merged by immunofluorescence (Figure 1D and H). Quantitatively, the mean number of spots of H3K4me3/H3K9ac, H3K4me3/RNAPII and H3K4me3/H3K9me3 was 22.9, 25.9 and 2.4 per nucleus, respectively (Figure 1I). Therefore, the coexistence of epigenetic marks was visualized at the single cell level by applying the *in situ* PLA, and this method was designated as iChmo.

Next, we analyzed whether iChmo can also detect a combination of two marks at a different histone protein of the same or neighboring nucleosomes within 30 nm, such as H3 and H4. By immunofluorescence using antibodies against H3K9me3 and H4K20me3, epigenetic marks for heterochromatin, their colocalization was confirmed by the presence of merged signals (Figure 1C). By iChmo using the same two antibodies, a large number of spots were produced (Figure 1G), and the mean number of spots was 72.5 per nucleus (Figure 1I), indicating that iChmo can visualize a combination of epigenetic marks, even if they are at different histone proteins in a close proximity.

Bivalent modification is specifically visualized at the single cell level

We focused on bivalent modification because of its biological significance and applied iChmo to visualize it using mouse ESCs and MEFs that have a lot of and few, respectively, bivalent modifications (3,5). By immunofluorescence staining of ESCs, H3K4me3 signals were observed as interspersed small dots, whereas H3K27me3 signals were enriched at the periphery of the nuclear membrane (Figure 2A). Some signals were merged in the nucleus, appearing to reflect the presence of bivalent modification. However, the same staining pattern was observed in MEFs (Supplementary Figure S1), and it was shown that immunofluorescence was not capable of distinguishing whether H3K4me3 and H3K27me3 were in close proximity. However, notably, by iChmo, a large number of fluorescence spots were observed in ESCs, whereas only a small number of spots were in MEFs (Figure 2B). This demonstrated that iChmo can distinguish whether two modifications coexist in the vicinity at the single cell level.

iChmo signals of bivalent modification are decreased in MEFs and Suz12 KO ESCs

To further confirm that iChmo signals originated from bivalent modification, we performed iChmo using *Suz12* KO ESCs. Suz12 is a component of Polycomb repressive complexes 2 together with Ezh2 and Eed (19), and is required for Polycomb repressive complexes 2 enzymatic activity (20). In the *Suz12* KO ESCs, global loss of H3K27me3 was observed by western blotting (15) and by immunofluorescence (Supplementary Figure S1), and loss of genomic regions with bivalent modification by quantitative ChIP-PCR (Supplementary Figure S2). iChmo produced no or few fluorescence spots of bivalent modification in the nucleus of *Suz12* KO ESCs (Figure 2B). The fact that this technique itself worked even in *Suz12* KO ESCs and MEFs was confirmed by detecting the coexistence of H3K4me3/H3K9ac and H3K4me3/RNAPII in these cells (Supplementary Figure S3). Quantitatively, the mean number of spots from bivalent modification was 0.9 and 4.1 per nucleus in the *Suz12* KO ESCs (69 nuclei counted) and MEFs (60 nuclei counted), respectively, whereas it was 15.2 in wild-type (WT) ESCs (58 nuclei counted) (Figure 2C). These data clearly showed that application of iChmo enabled us to visualize the bivalent modifications at the single cell level.

iChmo reveals highly concerted epigenetic changes during ESC differentiation

We took advantage of an imaging method to analyze individual cells in a heterogeneous sample, namely, ESCs at an early stage of differentiation. ESC differentiation was induced by all-trans RA treatment 24 h after removal of LIF and feeder layer cells. The expression of *Oct-4* mRNA decreased to the half 24 h after the RA treatment, but was still detectable 48 h after the treatment (Figure 3A). At cellular level, Oct-4 protein was detectable in all ESCs before the treatment but was heterogeneously detectable 24 h later (Figure 3B). At 48 h, in accordance with the residual *Oct-4* mRNA expression, a minor fraction of ESCs still had the Oct-4 protein expression (Figure 3B). ßIII-tubulin, a differentiated neuron marker, was also expressed in only a fraction of the ESCs (Figure 3B), showing the presence of large variations in the phenotypic

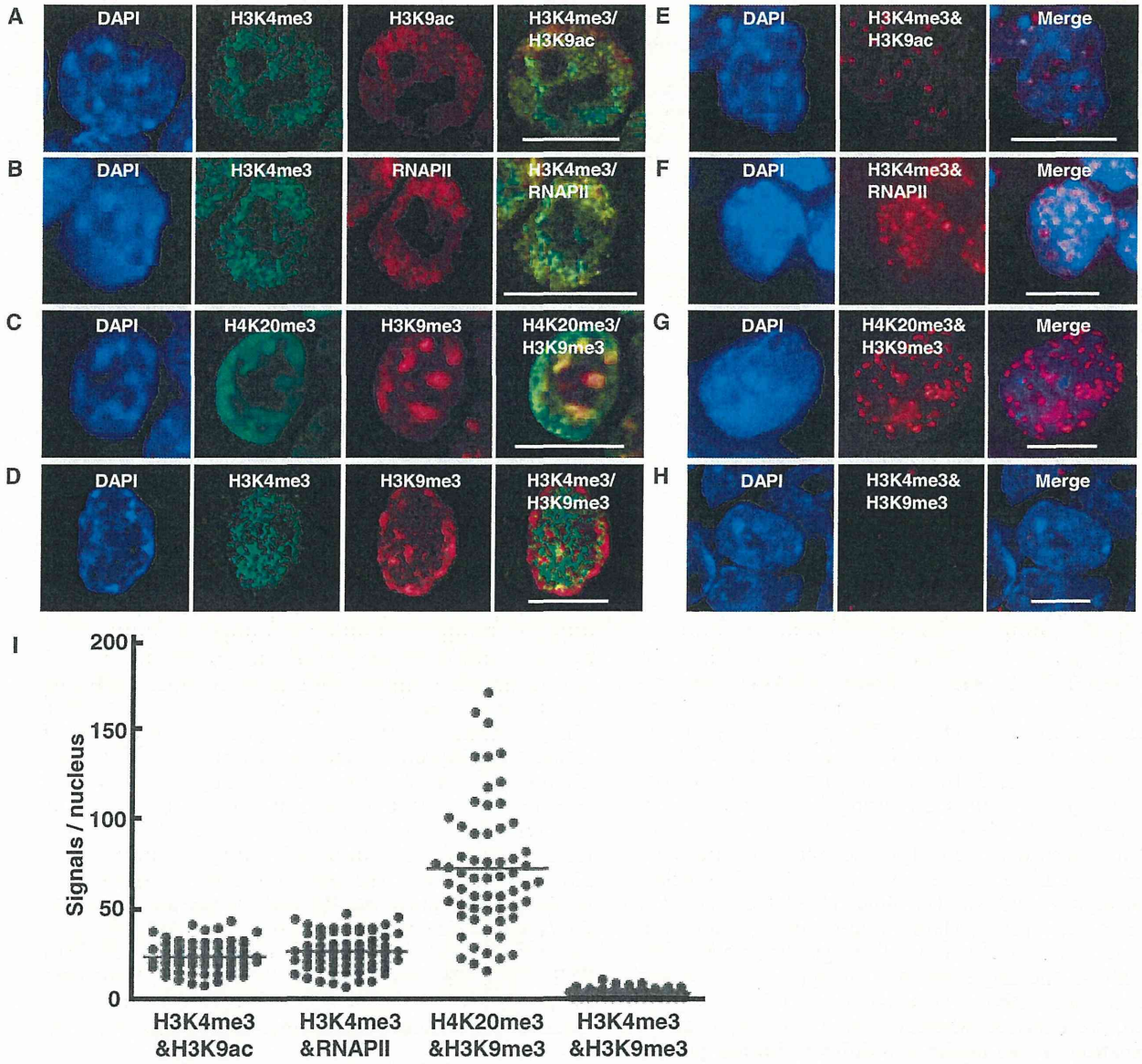

Figure 1. Visualization of combinations of epigenetic modifications in a single cell. Immunofluorescence staining was performed using mouse ESCs and antibodies against H3K4me3 and H3K9ac (**A**), H3K4me3 and RNAPII (**B**), H4K20me3 and H3K9me3 (**C**) and H3K4me3 and H3K9me3 (**D**). Colocalizations of H3K4me3/H3K9Ac, of H3K4me3/RNAP2 and of H4K20me3/H3K9me3 were observed, whereas that of H3K4me3/H3K9me3 was not. iChmo was performed using mouse ESCs and antibodies against H3K4me3 and H3K9ac (**E**), H3K4me3 and RNAPII (**F**), H4K20me3 and H3K9me3 (**G**) and H3K4me3 and H3K9me3 (**H**). Coexistence of H3K4me3/H3K9ac, of H3K4me3/RNAPII and of H4K20me3/H3K9me3, but not of H3K4me3/H3K9me3, was observed. Scale bar represents 10 μm. (**I**) The number of iChmo spots was counted for individual combinations in the nuclei of ESCs (H3K4me3 and H3K9ac, $n = 71$; H3K4me3 and RNAPII, $n = 70$; H4K20me3 and H3K9me3, $n = 60$; and H3K4me3 and H3K9me3, $n = 80$).

differentiation of the ESCs. In contrast, no or little fluorescence spots of the bivalent modification were observed 24 and 48 h after the RA treatment by iChmo, regardless of whether ESCs formed colonies or were differentiated into neuron-like cells (Figure 3C). The mean number of spots of ESCs at 48 h after the RA treatment was at the same level as that of the *Suz12* KO ESCs (Figure 3D). These data indicated that the epigenetic layer of differentiation was completed at 2 days in a highly concerted manner, whereas the phenotypic layer of differentiation proceeded with considerable variation.

iChmo visualizes a combination of histone modifications in tissue samples

If histone combinations in individual cells can be analyzed in tissues, this will enable us to identify cell populations of unique functions, such as stem cells. To apply iChmo to a

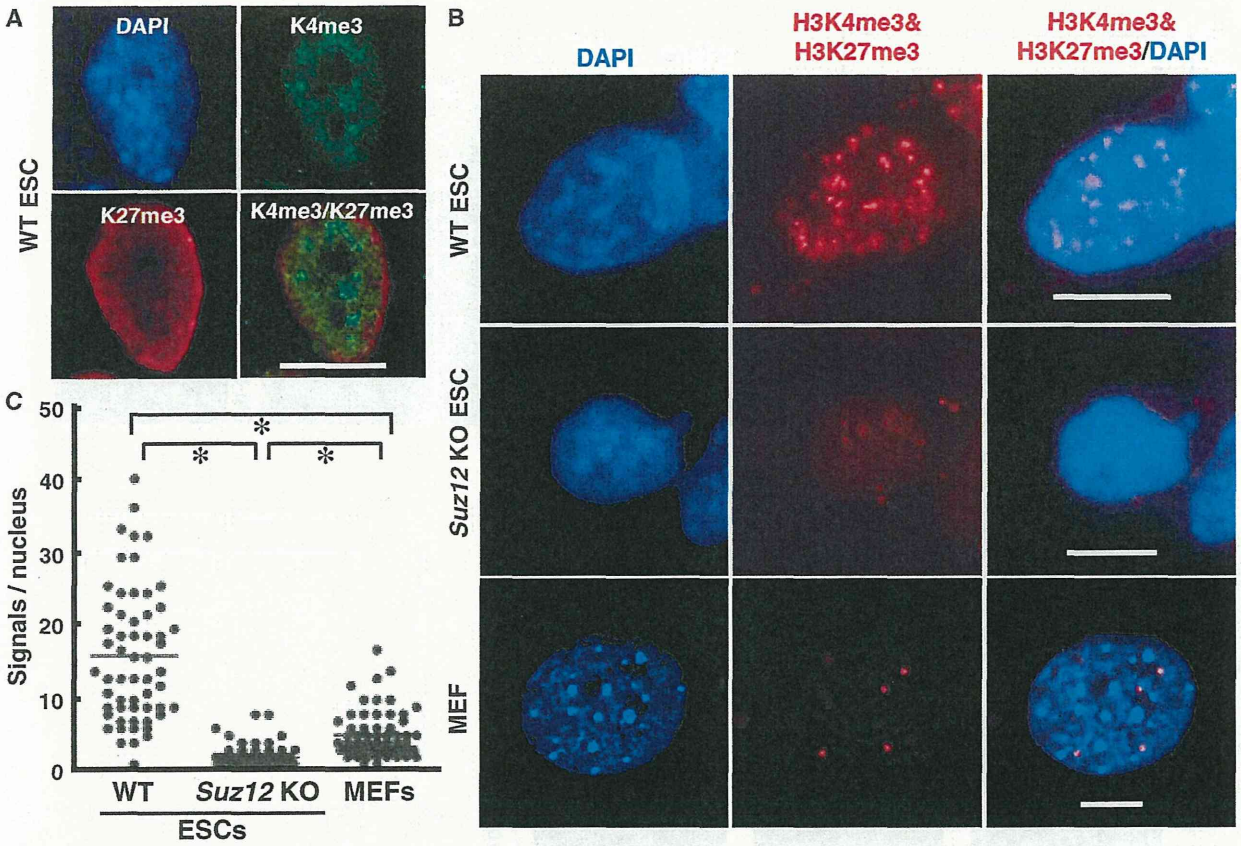

Figure 2. Application of iChmo to visualization of bivalent modification. (**A**) Mouse ESCs were stained by immunofluorescence with antibodies against H3K4me3 and H3K27me3 (scale bar: 10 μm). (**B**) Coexistence of H3K4me3 and H3K27me3 in WT ESCs was detected by iChmo, but hardly in *Suz12* KO ESCs and MEFs (scale bar: 10 μm). (**C**) The mean number of fluorescence spots was significantly larger in WT ESCs (15.2; $n = 58$) than in *Suz12* KO ESCs (0.9; $n = 69$) and MEFs (4.1; $n = 60$) (Mann–Whitney U-test; $^*P < 0.001$).

human tissue sample, we first screened 11 antibodies that had high specificity applicable to iChmo using cultured cells and identified that a combination of antibodies against H3K9me3 and H4K20me3 could be used for tissues samples (Figure 4A and B). Small dots of H3K9me3 were detected in all the cells of a human colonic tissue, presenting a similar staining pattern to that of cultured cells. Signals of H4K20me3 were also detected, and small dots of H3K9me3 were merged with those of H4K20me3 (Figure 4B). By iChmo, fluorescence spots were observed (Figure 4C) and were localized in the nuclei of cells (Figure 4D). Notably, the appearance of iChmo spots of H3K9me3 and H4K20me3 showed heterogeneity among the cells, and the cells that lacked iChmo spots corresponded to those that had strong DAPI intensity (Figure 4C and Supplementary Figure S4A and B), indicating that the presence of a combination of H3K9me3 and H4K20me3 was dependent on a cell condition, such as the cell cycle. The possibility that fluorescence spots were produced by non-specific binding of PLA probes was excluded by the absence of iChmo spots (Supplementary Figure S4E) using antibodies against H3K9ac and H4K20me3 (Supplementary Figure S4C and D).

DISCUSSION

An imaging method for a combination of epigenetic modifications in close proximity was established and was designated as iChmo. It had the capacity to visualize the combinations at the single cell level and thus was able to analyze heterogeneous samples, such as a cell line consisting of cells at various differentiation stages and tissue samples.

The application of iChmo to ESCs at their differentiation revealed that the epigenetic layer of differentiation takes place in a highly concerted manner before the phenotypic layer of differentiation. Previous reports showed that gene expression changes at several genes occur in parallel with histone modification changes during ESC differentiation (21,22). In addition, it is reported that, at *Hoxa1* and *Sox21*, development-related genes marked with bivalent modification, H3K27me3 levels decreased before gene activation at the early stage of ESC differentiation (23,24). However, up to now, it has been impossible to analyze to what degree such histone modification changes are concerted among cells during ESC differentiation, and the use of iChmo revealed highly concerted change. Also, taking advantage of its

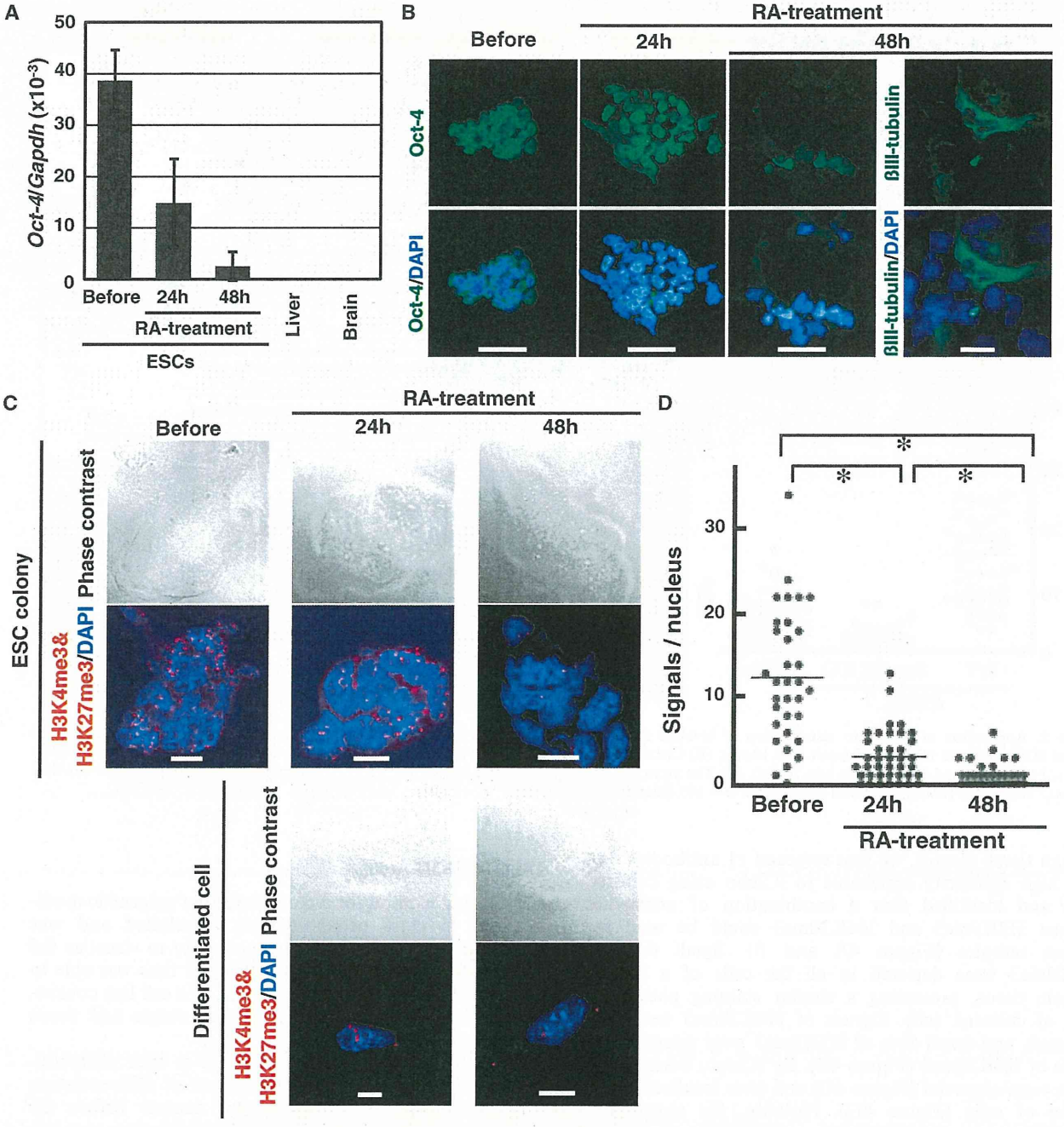

Figure 3. Visualization of epigenetic and phenotypic layers of differentiation in an early stage of ESC differentiation. (**A**) Differentiation of ESCs was induced by treatment of all-trans RA, and *Oct-4* mRNA expression was measured before, and 24 and 48 h after the RA treatment. The expression levels in the mouse liver and brain are shown as those in *Oct-4*-negative tissues. Values show mean + SD of three experiments. (**B**) Expression of Oct-4 and ßIII-tubulin proteins was analyzed in ESCs before, and 24 and 48 h after the RA treatment by immunofluorescence (scale bar: 20 µm). (**C**) Images of phase contrast and iChmo for the bivalent modification in ESC colonies before, and 24 and 48 h after the RA treatment (upper panel), and differentiated neuron-like cells at 24 and 48 h (lower panel). Regardless of the phenotypic differentiation statuses, the bivalent modification was absent both at 24 and 48 h, supporting highly concerted regulation of epigenetic changes. Scale bar represents 10 µm. (**D**) The number of fluorescence spots was counted in ESCs before ($n = 33$), and 24 ($n = 37$) and 48 ($n = 38$) h after the RA treatment (Mann–Whitney *U*-test; $*P < 0.001$). Although the decrease of Oct-4 expression and increase of ßIII-tubulin were highly variable among the ESCs treated with RA, the decrease of the bivalent modification was highly coordinated.

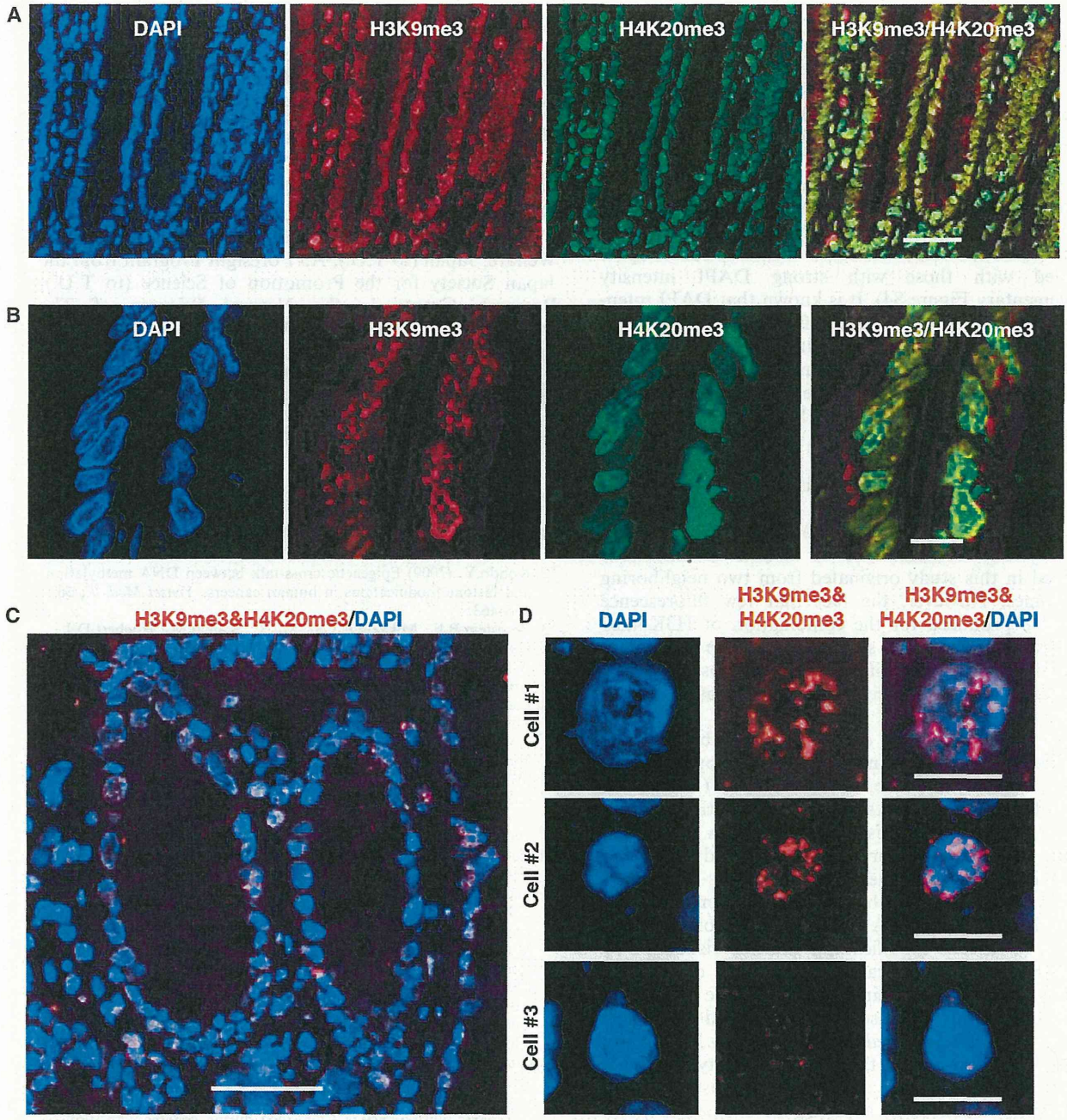

Figure 4. Application of iChmo to the analysis of human colonic tissue. (**A**) Human colonic tissues were stained by immunofluorescence with antibodies against H3K9me3 and H4K20me3 (scale bar: 50 μm). Colocalization of H3K9me3/ H4K20me3 was observed in the cells of colonic tissue. (**B**) High-magnification images of (A) (scale bar: 10 μm). (**C**) Coexistence of H3K9me3 and H4K20me3 was visualized in the nuclei of cells as fluorescence spots (scale bar: 50 μm). (**D**) High-magnification images of (C) (scale bar: 10 μm). The cells with iChmo spots (Cell #1 and #2) coincided with the cells having weak DAPI intensity, and the cells without iChmo spots (Cell #3) showed strong DAPI intensity.

applicability to a heterogeneous cell population and the role of bivalent modification in 'stemness', iChmo might be able to evaluate the level of cell reprogramming and the quality of iPS cells (25).

iChmo is also used for analysis of tissue sections. Although we analyzed only a limited number of combinations of histone modifications for now owing to availability of specific antibodies, analysis of tissue samples is expected to produce rich information, such as localization of tissue stem cells. Indeed, Lien *et al.* (4) clearly showed that the combination of H3K4me3 and H3K79me2 was specifically found in quiescent hair follicle

stem cells by ChIP-sequencing. We can expect that, by using iChmo, the presence of such combination of histone modifications can be demonstrated in a small amount of cells of histological sections. Also, aberrant expression of histone modifiers is now becoming evident in human disorders, especially in cancers (26), and iChmo might clarify which aberrant combinations are present, even if the fraction of cells with such aberrant combinations is small.

Analysis of human colonic tissue samples revealed the presence of heterogeneity of iChmo spots of H3K9me3 and H4K20me3, and the cells without iChmo spots coincided with those with strong DAPI intensity (Supplementary Figure S4). It is known that DAPI intensity is affected by DNA content, reflecting the phase of the cell cycle. In addition, considering that the levels of H3K9me3 and H4K20me3 dynamically change during the cell cycle (27), we can speculate that the heterogeneity of iChmo spots of H3K9me3 and H4K20me3 reflects the difference of the phases of the cell cycle.

The maximum distance between the primary antibodies recognized by two PLA probes has been estimated to be ~30 nm (14), which is longer than the minimum distance between two nucleosomes (~15 nm). Thus, there remains a possibility that combinations of histone modifications visualized in this study originated from two neighboring nucleosomes. However, the fact that few fluorescence spots were produced for the combination of H3K4me3 and H3K27me3 in MEFs supported that the signals are produced from two modifications at a close distance, theoretically within two neighboring nucleosomes.

iChmo showed a large number of spots of bivalent modification in ESCs, but only a small number of spots in MEFs, which was in line with a report by Bernstein *et al.* (3). At the same time, Mikkelsen *et al.* (5) reported that a half of bivalent marks in mouse ESCs still remained in MEFs. The apparent discrepancy between the iChmo data and the previous report can be accounted for by two possibilities; (i) because one iChmo spot does not always reflect one combination of histone modifications owing to the principle of *in situ* PLA (14), and all regions with coexistence of histone modifications are not visualized by this method, and (ii) because the number of bivalent marks is different according to the culture period of MEFs. In this study, we used MEFs cultured at passage five, whereas Mikkelsen *et al.* (5) used primary MEFs, and the authors also suggested the latter possibility.

To summarize, a specific combination of histone modifications was visualized by applying the *in situ* PLA, and the method was capable of analyzing heterogeneous cell population and tissue samples. Application of the method has the potential to uncover previously unknown biological and pathological significances of combinations of histone modifications.

SUPPLEMENTARY DATA

Supplementary Data are available at NAR Online: Supplementary Table 1, Supplementary Figures 1–4, Supplementary Methods and Supplementary Reference [28].

ACKNOWLEDGEMENTS

The authors thank Dr K. Shiota (The University of Tokyo) for providing them MEFs, and Drs T. Imai and N. Uchiya, and National Cancer Center Research Core Facility for the preparation of human tissues sections.

FUNDING

Grant-in-Aid for the Third-Term Comprehensive Cancer Control Strategy from the Ministry of Health, Labour and Welfare, Japan (to T.U.); A3 Foresight Program from the Japan Society for the Promotion of Science (to T.U.); Research Grants in the Natural Sciences of The Mitsubishi Foundation (to T.U. and N.H.). Funding for open access charge: Third-Term Comprehensive Cancer Control Strategy from the Ministry of Health, Labour and Welfare, Japan.

Conflict of interest statement. None declared.

REFERENCES

1. Meissner,A. (2010) Epigenetic modifications in pluripotent and differentiated cells. *Nat. Biotechnol.*, **28**, 1079–1088.
2. Kondo,Y. (2009) Epigenetic cross-talk between DNA methylation and histone modifications in human cancers. *Yonsei Med. J.*, **50**, 455–463.
3. Bernstein,B.E., Mikkelsen,T.S., Xie,X., Kamal,M., Huebert,D.J., Cuff,J., Fry,B., Meissner,A., Wernig,M., Plath,K. *et al.* (2006) A bivalent chromatin structure marks key developmental genes in embryonic stem cells. *Cell*, **125**, 315–326.
4. Lien,W.H., Guo,X., Polak,L., Lawton,L.N., Young,R.A., Zheng,D. and Fuchs,E. (2011) Genome-wide maps of histone modifications unwind in vivo chromatin states of the hair follicle lineage. *Cell Stem Cell*, **9**, 219–232.
5. Mikkelsen,T.S., Ku,M., Jaffe,D.B., Issac,B., Lieberman,E., Giannoukos,G., Alvarez,P., Brockman,W., Kim,T.K., Koche,R.P. *et al.* (2007) Genome-wide maps of chromatin state in pluripotent and lineage-committed cells. *Nature*, **448**, 553–560.
6. Rada-Iglesias,A., Bajpai,R., Swigut,T., Brugmann,S.A., Flynn,R.A. and Wysocka,J. (2011) A unique chromatin signature uncovers early developmental enhancers in humans. *Nature*, **470**, 279–283.
7. Xiao,S., Xie,D., Cao,X., Yu,P., Xing,X., Chen,C.C., Musselman,M., Xie,M., West,F.D., Lewin,H.A. *et al.* (2012) Comparative epigenomic annotation of regulatory DNA. *Cell*, **149**, 1381–1392.
8. Ruthenburg,A.J., Li,H., Milne,T.A., Dewell,S., McGinty,R.K., Yuen,M., Ueberheide,B., Dou,Y., Muir,T.W., Patel,D.J. *et al.* (2011) Recognition of a mononucleosomal histone modification pattern by BPTF via multivalent interactions. *Cell*, **145**, 692–706.
9. Vastenhouw,N.L., Zhang,Y., Woods,I.G., Imam,F., Regev,A., Liu,X.S., Rinn,J. and Schier,A.F. (2010) Chromatin signature of embryonic pluripotency is established during genome activation. *Nature*, **464**, 922–926.
10. Roh,T.Y., Cuddapah,S., Cui,K. and Zhao,K. (2006) The genomic landscape of histone modifications in human T cells. *Proc. Natl Acad. Sci. USA*, **103**, 15782–15787.
11. Tsai,W.W., Wang,Z., Yiu,T.T., Akdemir,K.C., Xia,W., Winter,S., Tsai,C.Y., Shi,X., Schwarzer,D., Plunkett,W. *et al.* (2010) TRIM24 links a non-canonical histone signature to breast cancer. *Nature*, **468**, 927–932.
12. Geisberg,J.V. and Struhl,K. (2004) Quantitative sequential chromatin immunoprecipitation, a method for analyzing co-occupancy of proteins at genomic regions in vivo. *Nucleic Acids Res.*, **32**, e151.
13. Voigt,P., LeRoy,G., Drury,W.J. 3rd, Zee,B.M., Son,J., Beck,D.B., Young,N.L., Garcia,B.A. and Reinberg,D. (2012) Asymmetrically modified nucleosomes. *Cell*, **151**, 181–193.

14. Soderberg,O., Gullberg,M., Jarvius,M., Ridderstrale,K., Leuchowius,K.J., Jarvius,J., Wester,K., Hydbring,P., Bahram,F., Larsson,L.G. *et al.* (2006) Direct observation of individual endogenous protein complexes in situ by proximity ligation. *Nat. Methods*, **3**, 995–1000.
15. Pasini,D., Bracken,A.P., Hansen,J.B., Capillo,M. and Helin,K. (2007) The polycomb group protein Suz12 is required for embryonic stem cell differentiation. *Mol. Cell. Biol.*, **27**, 3769–3779.
16. Perez-Burgos,L., Peters,A.H., Opravil,S., Kauer,M., Mechtler,K. and Jenuwein,T. (2004) Generation and characterization of methyl-lysine histone antibodies. *Methods Enzymol.*, **376**, 234–254.
17. Kimura,H., Hayashi-Takanaka,Y., Goto,Y., Takizawa,N. and Nozaki,N. (2008) The organization of histone H3 modifications as revealed by a panel of specific monoclonal antibodies. *Cell Struct. Funct.*, **33**, 61–73.
18. Kim,T.H., Barrera,L.O., Qu,C., Van Calcar,S., Trinklein,N.D., Cooper,S.J., Luna,R.M., Glass,C.K., Rosenfeld,M.G., Myers,R.M. *et al.* (2005) Direct isolation and identification of promoters in the human genome. *Genome Res.*, **15**, 830–839.
19. Ku,M., Koche,R.P., Rheinbay,E., Mendenhall,E.M., Endoh,M., Mikkelsen,T.S., Presser,A., Nusbaum,C., Xie,X., Chi,A.S. *et al.* (2008) Genomewide analysis of PRC1 and PRC2 occupancy identifies two classes of bivalent domains. *PLoS Genet.*, **4**, e1000242.
20. Pasini,D., Bracken,A.P., Jensen,M.R., Lazzerini Denchi,E. and Helin,K. (2004) Suz12 is essential for mouse development and for EZH2 histone methyltransferase activity. *EMBO J.*, **23**, 4061–4071.
21. Lee,E.R., Murdoch,F.E. and Fritsch,M.K. (2007) High histone acetylation and decreased polycomb repressive complex 2 member levels regulate gene specific transcriptional changes during early embryonic stem cell differentiation induced by retinoic acid. *Stem Cells*, **25**, 2191–2199.
22. Feldman,N., Gerson,A., Fang,J., Li,E., Zhang,Y., Shinkai,Y., Cedar,H. and Bergman,Y. (2006) G9a-mediated irreversible epigenetic inactivation of Oct-3/4 during early embryogenesis. *Nat. Cell Biol.*, **8**, 188–194.
23. Chakravarthy,H., Ormsbee,B.D., Mallanna,S.K. and Rizzino,A. (2011) Rapid activation of the bivalent gene Sox21 requires displacement of multiple layers of gene-silencing machinery. *FASEB J.*, **25**, 206–218.
24. Lee,T.I., Jenner,R.G., Boyer,L.A., Guenther,M.G., Levine,S.S., Kumar,R.M., Chevalier,B., Johnstone,S.E., Cole,M.F., Isono,K. *et al.* (2006) Control of developmental regulators by Polycomb in human embryonic stem cells. *Cell*, **125**, 301–313.
25. Hanna,J.H., Saha,K. and Jaenisch,R. (2010) Pluripotency and cellular reprogramming: facts, hypotheses, unresolved issues. *Cell*, **143**, 508–525.
26. Chi,P., Allis,C.D. and Wang,G.G. (2010) Covalent histone modifications–miswritten, misinterpreted and mis-erased in human cancers. *Nat. Rev. Cancer*, **10**, 457–469.
27. Black,J.C., Van Rechem,C. and Whetstine,J.R. (2012) Histone lysine methylation dynamics: establishment, regulation, and biological impact. *Mol. Cell*, **48**, 491–507.
28. Takeshima,H., Yamashita,S., Shimazu,T., Niwa,T. and Ushijima,T. (2009) The presence of RNA polymerase II, active or stalled, predicts epigenetic fate of promoter CpG islands. *Genome Res.*, **19**, 1974–1982.

JJCO Japanese Journal of Clinical Oncology

Jpn J Clin Oncol 2013;43(6)641–645
doi:10.1093/jjco/hyt058
Advance Access Publication 25 April 2013

Stronger Prognostic Power of the CpG Island Methylator Phenotype than Methylation of Individual Genes in Neuroblastomas

Kiyoshi Asada[1], Naoko Watanabe[1], Yohko Nakamura[2], Miki Ohira[3], Frank Westermann[4], Manfred Schwab[4], Akira Nakagawara[2] and Toshikazu Ushijima[1,*]

[1]Division of Epigenomics, National Cancer Center Research Institute, Tokyo, [2]Division of Biochemistry and Innovative Cancer Therapeutics, Chiba Cancer Center Research Institute, [3]Laboratory of Cancer Genomics, Chiba Cancer Center Research Institute, Chiba, Japan and [4]Division of Tumor Genetics, German Cancer Research Center, Heidelberg, Germany

*For reprints and all correspondence: Toshikazu Ushijima, Division of Epigenomics, National Cancer Center Research Institute, 5-1-1 Tsukiji, Chuo-ku, Tokyo 104-0045, Japan. E-mail: tushijim@ncc.go.jp

Received January 14, 2013; accepted March 30, 2013

Objective: The CpG island methylator phenotype is strongly associated with poor survival in neuroblastomas. Neuroblastomas with the CpG island methylator phenotype include almost all neuroblastomas with *MYCN* amplification, and, even among neuroblastomas without *MYCN* amplification, have worse prognosis. At the same time, methylation of individual tumor-suppressor genes is also reported to be associated with poor survival. The purpose of this study was to compare the prognostic power of the CpG island methylator phenotype with that of methylation of individual genes.

Methods: Methylation-specific polymerase chain reaction was performed for five individual genes (*CASP8*, *EMP3*, *HOXA9*, *NR1I2* and *CD44*) in 140 Japanese and 152 German neuroblastomas. Kaplan–Meier analysis and log-rank tests were conducted to compare the survival between groups defined by methylation status.

Results: Among the five individual genes, only *CASP8* methylation had a significant association with poor overall survival both in Japanese (hazard ratio = 3.1; 95% confidence interval = 1.5–6.4; $P = 0.002$) and German (hazard ratio = 4.8; 95% confidence interval = 2.1–11; $P = 0.0002$) neuroblastomas. *HOXA9* and *NR1I2* methylation were associated with poor survival only in German neuroblastomas. On the other hand, the CpG island methylator phenotype had a strong and consistent association in Japanese (hazard ratio = 22; 95% confidence interval = 5.3–93; $P = 1.5 \times 10^{-5}$) and German (hazard ratio = 9.5; 95% confidence interval = 3.2–28; $P = 4.7 \times 10^{-5}$) neuroblastomas.

Conclusion: The CpG island methylator phenotype is likely to have stronger prognostic power than methylation of individual genes in neuroblastomas.

Key words: neuroblastoma – methylation – CIMP – poor survival

INTRODUCTION

Neuroblastoma (NBL) is the most frequent extracranial pediatric tumor (1). The CpG island methylator phenotype (CIMP), methylation of multiple CpG islands (CGIs), was associated with poor survival with a hazard ratio (HR) of 22 [95% confidence interval (95% CI) = 5.3–93] in Japanese and 9.5 (95% CI = 3.2–28) in German NBLs, respectively (2,3). The prognostic significance of CIMP was further confirmed in Italian NBLs by a pyrosequencing assay (4). Notably, NBLs with CIMP included almost all NBLs with *MYCN* amplification (37/38 in Japanese and 23/23 in German NBLs), the strongest current prognostic marker (5–7). Even among NBLs without

MYCN amplification, CIMP was a significant and strong prognostic marker with an HR of 12 (95% CI = 2.6–59) in Japanese and 4.5 (95% CI = 1.3–16) in German NBLs.

CIMP is sensitively detected by methylation of marker CGIs, such as CGIs in gene bodies of the *PCDHB* gene family in NBLs. It is known that methylation of CGIs outside promoter regions (non-promoter CGIs) is not associated with loss of expression, and such non-promoter CGIs are more susceptible to methylation induction than promoter CGIs (8). As a model of the close association between methylation of non-promoter CGIs and poor survival, it was considered that CIMP consistently leads to methylation of non-promoter CGIs, such as CGIs of the *PCDHB* gene family in NBLs, and also to methylation of various promoter CGIs with low incidences, which causes poor survival.

At the same time, methylation of an individual gene has been also shown to be associated with poor survival. For example, methylation of *CASP8* was associated with poor survival with an HR of 5.3 (95% CI = 1.5–18; $P = 0.008$) (9). Methylation of *NR1I2*, *EMP3*, *HOXA9* and *CD44* was associated with poor survival with P values of 0.014, 0.03, 0.04 and 0.049, respectively (9–12). Functionally, *CASP8*, an apoptosis-related gene, has been reported to act as a tumor suppressor, and its loss is required for survival of NBL cells overexpressing *MYC* or *MYCN* (13). *NR1I2* (a nuclear receptor gene) and *EMP3* (a myelin-related gene) have been reported to have growth suppressive activity in NBL cells (10,11). However, the prognostic powers of methylation of these individual genes and of CIMP have never been analyzed in identical sets of NBLs.

In the present study, we aimed to compare the prognostic power of CIMP with that of methylation of individual genes.

PATIENTS AND METHODS

DNA Samples and Analysis of CIMP

The 140 Japanese and 152 German NBLs were identical with those analyzed in our previous studies (2,3). These samples were analyzed at the Division of Epigenomics, National Cancer Center Research Institute under the approval of institutional review boards. The presence of CIMP and *MYCN* amplification were determined as in our previous studies (2,3), and this information was used in the present study.

Sodium Bisulfite Modification and Methylation-specific Polymerase Chain Reaction (PCR)

Fully methylated DNA and fully unmethylated DNA were prepared by methylating genomic DNA with *Sss*I methylase (New England Biolabs, Beverly, MA, USA) and by amplifying genomic DNA with the GenomiPhi amplification system (GE Health Care, Buckinghamshire, UK), respectively. Bisulfite modification was performed using 1 μg of *Bam*HI-digested genomic DNA as previously described (14), and the modified DNA was suspended in 40 μl of Tris–ethylenediaminetetraacetic acid buffer (pH 8.0). An aliquot of 1 μl was used for methylation-specific PCR (MSP).

MSP was performed using primers as previously published (11,13,15,16) (Supplementary data, Table S1). For the *NR1I2* gene, although the combined bisulfite restriction analysis was performed in the previous study (10), MSP targeting the same region was used in this study. Using fully methylated and unmethylated DNA, the annealing temperature that specifically amplified only methylated or unmethylated DNA was determined. Also, a minimum number of PCR cycles to obtain visible bands was determined using the (un)methylated DNA, and four cycles were added for the analysis of primary NBLs (Supplementary data, Table S1).

Statistical Analysis

Survival time was defined as the time between initial diagnosis and death, or time between diagnosis and last contact if no event had occurred. Kaplan–Meier analysis and log-rank tests were conducted to compare survival between the groups defined by methylation status. HRs were estimated by the Cox

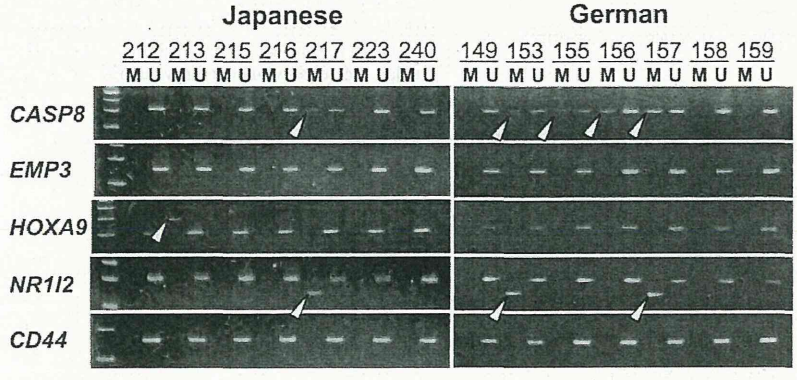

Figure 1. Methylation of promoter CpG islands (CGIs) of five individual genes (*CASP8*, *EMP3*, *HOXA9*, *NR1I2* and *CD44*) in Japanese and German neuroblastomas (NBLs). Representative results of methylation-specific PCR are shown. M and U, primers specific to methylated and unmethylated DNA, respectively. Arrowheads show the presence of methylated DNA molecules.

proportional hazard model. These statistical analyses were performed using the SPSS software, version 13.0 (SPSS Inc., Chicago, IL, USA).

RESULTS

Methylation of Individual Genes and their Prognostic Power Compared with CIMP

CASP8, *EMP3*, *HOXA9*, *NR1I2* and *CD44* were methylated in 26, 4, 27, 15 and 3, respectively, of the 140 Japanese NBLs, and in 30, 2, 2, 13 and 2, respectively, of the 152 German NBLs (representative results shown in Fig. 1). The prognostic power of methylation of the five genes was analyzed in Japanese and German NBLs, respectively (Fig. 2A and Table 1). In Japanese NBLs, only *CASP8* methylation had a significant association with poor survival (HR = 3.1; 95% CI = 1.5–6.4; $P = 0.002$). Regarding CIMP, defined by methylation of multiple genes and detected by methylation of the *PCDHB* gene family (2), it had a strong association with poor survival (HR = 22; 95% CI = 5.3–93; $P = 1.5 \times 10^{-5}$), and its prognostic power was stronger than that of *MYCN* amplification (HR = 9.5; 95% CI = 4.4–21; $P = 4.0 \times 10^{-9}$) (Fig. 2B). In the identical set of Japanese NBLs, a stronger prognostic power of CIMP than methylation of an individual gene was clearly shown.

In German NBLs, *CASP8* methylation was also associated with poor survival (HR = 4.8; 95% CI = 2.1–11; $P = 0.0002$) (Fig. 2A and Table 1). In addition, *HOXA9* and *NR1I2* methylation were associated with poor survival with an HR of 14 for *HOXA9* (95% CI = 3.1–62; $P = 0.0006$) and 4.2 for *NR1I2* (95% CI = 1.6–11; $P = 0.003$), respectively. Regarding CIMP and *MYCN*, as shown in our previous study (3), CIMP had a strong association with poor survival (HR = 9.5; 95% CI = 3.2–28; $P = 4.7 \times 10^{-5}$) and it was comparable to that of *MYCN* (HR = 12; 95% CI = 4.9–29; $P = 4.8 \times 10^{-8}$) (Fig. 2B). The stronger prognostic power of CIMP was consistently shown in the identical set of German NBLs.

Association Between CIMP and Methylation of Individual Genes

Among the five individual genes analyzed in this study, two genes (*CASP8* and *NR1I2*) were methylated at a significantly higher incidence in NBLs with CIMP (Fig. 3). In Japanese NBLs with and without CIMP, *CASP8* methylation was found in 24/67 and 2/73, respectively ($P = 5.0 \times 10^{-7}$). *NR1I2* methylation was found in 15/67 and 0/73, respectively ($P = 3.2 \times 10^{-5}$). Also in German NBLs with and without CIMP, *CASP8* methylation was found in 28/50 and 2/95, respectively ($P = 2.6 \times 10^{-14}$). *NR1I2* methylation was found in 11/50 and 1/95, respectively ($P = 1.4 \times 10^{-5}$). These results showed that CIMP was associated with methylation of multiple promoter CGIs, mainly *CASP8* and *NR1I2*.

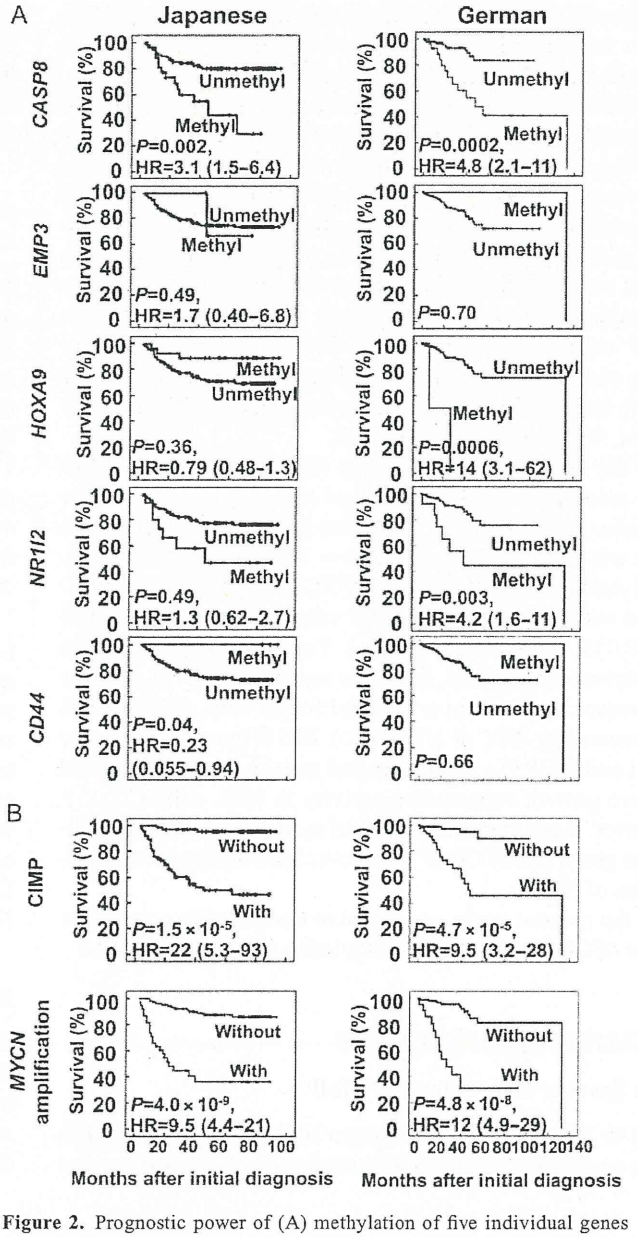

Figure 2. Prognostic power of (A) methylation of five individual genes (*CASP8*, *EMP3*, *HOXA9*, *NR1I2* and *CD44*), and (B) CpG island methylator phenotype (CIMP) and MYCN amplification in Japanese and German NBLs. Kaplan–Meier survival curves were drawn using the SPSS software. Among the five genes, only CASP8 methylation had a significant association with poor survival both in Japanese and German NBLs.

DISCUSSION

The stronger prognostic power of CIMP than methylation of individual genes was shown in this study. Also, the association between CIMP and methylation of multiple promoter CGIs was indicated. These results supported the idea that CIMP leads to a poor prognosis by induction of methylation of promoter CGIs of various tumor-suppressor genes with low incidences.